

Defect-induced magnetically-sensitive valley polarization reversal and revival in WSe₂-WS₂ heterostructure

Taishen Li^{1,‡}, Tao Yu^{2,‡}, Xuefeng Cui¹, Kaixuan Zhang¹, Jianyi Liu¹, Qiushi Meng¹, Hongbing Cai^{1,3}, Nan Pan^{1,3,*}, Bing Wang^{1,3}, Zhenchao Dong¹ and Xiaoping Wang^{1,3,*}

¹*Hefei National Laboratory for Physical Sciences at the Microscale, University of Science and Technology of China, Hefei, Anhui 230026, P.R. China,*

²*Kavli Institute of NanoScience, Delft University of Technology, 2628 CJ Delft, The Netherlands*

³*Key Laboratory of Strongly-Coupled Quantum Matter Physics, Chinese Academy of Sciences, School of Physical Sciences, University of Science and Technology of China, Hefei, Anhui 230026, P. R. China. ‡These authors contributed equally to this work.*

*Correspondence and requests for materials should be addressed to X. P. W. (email:

xpwang@ustc.edu.cn) or to N. P (email: npan@ustc.edu.cn).

Abstract

Manipulating and reserving the valley pseudospin of excitons are one core aim in the transition metal dichalcogenides (TMDs). However, due to the strong electron-hole exchange and spin-orbit coupling interactions, the exciton recombination lifetime is subject to picosecond timescale intrinsically, and the valley polarization is hardly modulated by the moderate magnetic field. It is fortunate that interlayer and defect-localized excitons promise to overcome these difficulties by suppressing these interactions. Here we clearly reveal that the valley polarization can be reversed and revived in the defect-localized excitons with microsecond lifetime in AB-stacked WSe₂-WS₂ heterobilayer. Specifically, for the interlayer defect-localized exciton, the valley polarization is reversed and can be enhanced efficiently by a weak out-of-plane magnetic field ($< \pm 0.4\text{T}$). In sharp contrast, for the intralayer defect-localized exciton, the valley polarization can revive after a fast relaxation process whose sign follows the direction of a strong out-of-plane magnetic field ($> \pm 1\text{T}$). We explain the reversed valley polarization with magnetic-field sensitivity by the delocalization of defect-localized holes by a weak magnetic field and the revival of valley polarization by the valley Zeeman effect from a strong magnetic field. Our results raise the prospect to find rich and novel valley dynamics in defect-localized excitons in the TMDs heterobilayer.

Introduction

The electronic, optical and magnetic properties of the atomically thin transition metal dichalcogenides (TMDs) in the MX₂ (M=Mo, W; X=S, Se) have been studied intensively in the past few years¹. For monolayer TMDs, benefiting from the strong spin-orbit interaction and broken inversion symmetry, the spin and valley degrees of freedom are coupled to each other, enabling a circular optical access to the valley pseudospin by the valley-dependent optical selection rules². Using the valley pseudospin coupled with the excitonic states, the TMDs have emerged as promising

candidates for storing, encoding and proceeding information. However, owing to the strong electron–hole exchange interactions in monolayer TMDs, the valley polarization lifetime is intrinsically limited to picosecond³. Such short valley polarization lifetime seriously limits the development of valleytronic devices that should allow the manipulation of the valley pseudospin before its dissipation or decoherence in monolayer TMDs. Therefore, constructing architectures with higher valley polarization and longer valley lifetime holds the key for practical applications.

Fortunately, it has been proposed very recently that the TMDs' van der Waals (vdW) heterostructures, realized by either viscoelastic stamping or heteroepitaxial growth of two different monolayer TMDs, possess the unique advantages to circumvent these limitations⁴⁻⁵. Specifically, for type II band alignment, electrons and holes find their energy minimums in different layers⁶ and the spatial separation reduces the overlap of electron and hole wavefunctions and changes the exciton properties significantly⁷. Moreover, in this heterobilayer configuration, it allows to engineer the valley properties of the interlayer exciton by tuning a series of degrees of freedom, such as changing the geometric arrangement of bilayer stacking, selecting different TMDs as the components, imposing an external electric field and so on⁸⁻¹⁰. In parallel, it has also been demonstrated very recently that, defects in monolayer TMDs could be exceptionally desirable for various desired properties¹¹⁻¹⁴, and the excitons localized at which can behave as single-photon emitters¹⁵⁻¹⁶, and/or possess a microsecond valley lifetime¹⁷. Thus, it is natural to ask: if a heterobilayer of TMDs was composed of the monolayers with certain defects, could these intralayer defects play any role in tuning the valley properties of the interlayer exciton. As far as we know, such kind of study on the role of defects in the heterostructures of TMDs has not yet been explored.

In the present work, we have explored the magnetically-tunable valley dynamics of the defect-localized excitons in the AB stacked WSe₂-WS₂ heterostructure through both the steady-state and time-resolved photoluminescence (PL) measurements with polarization resolution. We have found that both the interlayer (IX_{def}) and intralayer (X_{def}) defect-localized excitons possess microsecond valley lifetimes, exhibiting intriguing magnetically-sensitive responses in their valley dynamics. On one hand, the valley polarization of IX_{def} is reversed and can be significantly enhanced by a weak out-of-plane magnetic field ($B_z < \pm 0.4\text{T}$), presenting a “Λ” pattern in the magnetic-field dependence. On the other hand, the valley polarization of X_{def} can revive after a fast relaxation process whose sign follows the direction of a strong out-of-plane magnetic field ($B_z > \pm 1\text{T}$) and exhibits an “X” pattern. We explain the magnetic-field-sensitive reversed valley polarization by the delocalization of defect-localized holes by a weak magnetic field that then hops to another layer to emit oppositely polarized light. While the revival of valley polarization in the intralayer exciton roots in the valley Zeeman effect from a strong magnetic field.

PL properties of defect-localized excitons in the heterostructure.

The monolayer flakes of WSe₂ and WS₂ used in this study were grown respectively onto the 300-nm-thick SiO₂/Si substrates by conventional chemical vapor deposition (CVD) method, and then were stacked to form the heterobilayers in an AB alignment

by a wet transfer method through polymethy methacrylate (PMMA)¹⁸ using a homemade high-precision transfer platform (see method section). The optical microscope image of an established heterostructure is displayed in Fig. 1a, the configuration of AB stacking can be easily recognized by the completely opposite arrangement of the two regular triangles. Fig. 1b shows the PL spectrum of monolayer WS₂, WSe₂ and heterostructure zones at temperature of 10 K excited by a laser with 532 nm wavelength and spot size about 1 μ m. From these PL spectra, we can figure out that the peak at 615 nm and 740 nm correspond to intralayer exciton of monolayer WS₂ and WSe₂, respectively. For the new arising peak at 860 nm, it is attributed to the interlayer exciton, in which electrons are in the lower conduction band of monolayer WS₂ and holes reside in the upper valence band of monolayer WSe₂^{4, 19-21}. In detail, we can clearly observe that the PL of WSe₂ monolayer includes two peaks (740 nm and 715 nm). As reported in the literature, the binding energy between excitons and trions is about 20~40 meV for TMDs generally²²⁻²⁴. Nevertheless, the calculated energy gap between the two peaks is about 58 meV, which is much larger than the binding energy of trions. Therefore, we infer the higher energy shoulder peak corresponds to intrinsic exciton of WSe₂, and the lower one comes from the defect-localized exciton (X_{def}). In order to obtain some more useful information, we collect the PL spectrum at different temperature (Fig. S1) and show the normalized PL of both 740 nm and 860 nm as a function of temperature and wavelength in Fig. 1c and d, respectively.

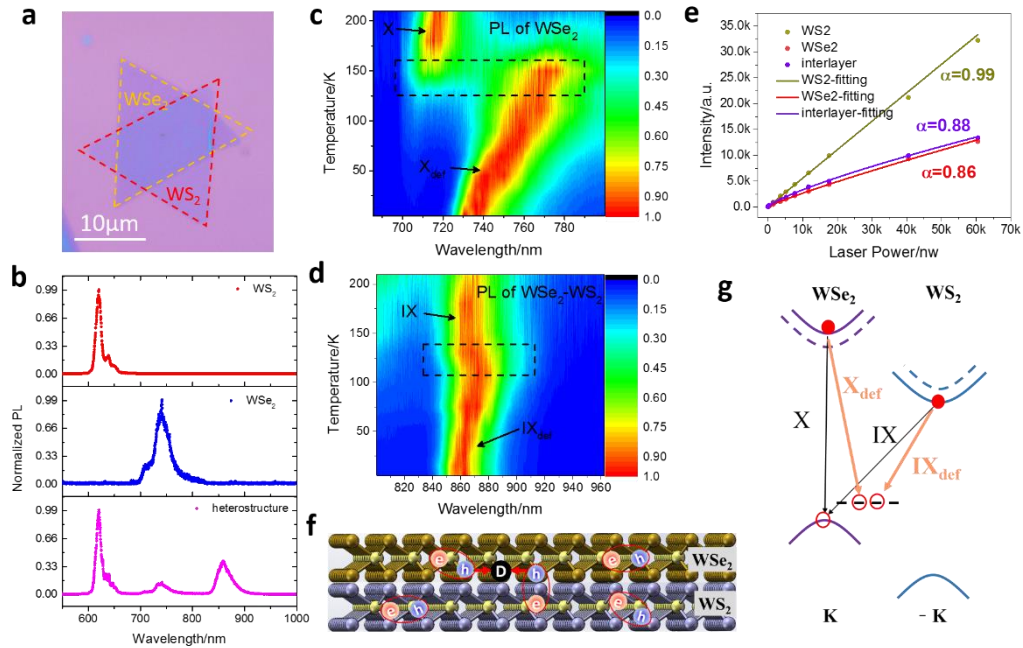


Fig. 1 PL properties and band alignment of AB-stacked WSe₂-WS₂ heterostructure. a, The optical microscope image of AB-stacked WSe₂-WS₂ heterostructure. b, Normalized PL properties of monolayer WS₂ zone (red curve), monolayer WSe₂ zone (blue curve) and heterostructure zone (purple curve) in the sample, respectively. c and d, Normalized PL spectrum corresponding to monolayer WSe₂ zone and heterostructure zone as a function of temperature, respectively. e, excitation power dependent PL properties, the colorful dots and lines correspond to experiment data and fitting results, respectively. f and g, schematics of exciton configuration in real space and band

alignment of AB-stacked WSe₂-WS₂ heterostructure.

From Fig. 1c and d, we can clearly observe that, unlike the usual monotonic redshift temperature dependence of an excitonic interband transition, the spectra of these two excitons share a common “transition point” roughly around 120 K (black dashed boxes in Fig. 1c and d). Both of the peaks redshift monotonically below this temperature range, whereas hop abruptly to the higher energies above the range. This “transition” feature comes from the thermal activation process from defect-bound to free excitons, which clearly indicates the defect-trapped natures of both the interlayer exciton and the WSe₂ intralayer one (X_{def}) especially at the low temperatures, and strongly suggests the same defect origin shared by IX_{def} and X_{def} . In order to further confirm the role of defects, we plot the PL intensity as a function of excitation power in Fig. 1e (color dots) and fit the experiment data using the formula $I=P^\alpha$, where I is the PL intensity, P is the excited laser power, and α represents the fitting constant. From the fitting results, we can observe that the PL located at 615nm presents a linear relation with excitation power ($\alpha \sim 0.99$), indicating the intrinsic exciton property of monolayer WS₂. However, the PL located at 740 nm and 860 nm show similar sub-linear dependence on the laser power ($\alpha \sim 0.86$ and 0.88 , respectively). Since IX_{def} and X_{def} share the same defect origin which comes unambiguously from the monolayer WSe₂, the defect level must be shallow-acceptor-like, exactly locating above the valence band maximum of the WSe₂¹². With all of these results, eventually we can clearly define the band alignment structure of the heterobilayer samples, as sketched in figure 1g.

Transition dynamics of defect-localized excitons in the heterostructure.

In order to explore the transition process of the defect related excitons, we further explore the time-resolved PL under different temperature using a pulse laser at 670 nm wavelength with light spot size $\sim 1 \mu\text{m}$. The experimental time-resolved PL spectra of monolayer WSe₂ and WSe₂-WS₂ heterobilayer are shown in Fig. 2a and b, respectively. From experimental results, we can clearly observe that the transitions of both excitons in Fig. 2a and b include the fast and slow processes. The slow process is significantly suppressed as the increasing temperature. Therefore, it is necessary to use the double exponential formula to fit the exciton dynamics of the fast and slow process. The fitting formula is in the form of²⁵

$$I(t) = A_1 e^{-\frac{t}{\tau_1}} + \frac{B}{t+R} + A_2 e^{-\frac{t}{\tau_2}}, \quad (1)$$

where τ_1 and τ_2 are the lifetimes of the fast and slow process, respectively. A_1 , A_2 , B and R are fitting parameters related to the initial population and the rate constants. Fig. 2c and d show typical fitting results for time-resolved PL of monolayer WSe₂ and WSe₂-WS₂ heterobilayer measured at temperature 5K, respectively. We can clearly observe that the time-resolved PL can be well fitted by the double exponential formula (equation 1). The fitting results of the initial population (A_1 and A_2) corresponding to spectra of monolayer WSe₂ and WSe₂-WS₂ heterobilayer are shown in Fig. S2a and c, respectively. From the experiment and fitting results, the initial population of the slow process is monotonously reduced (A_2), and even disappear at 180 K; however, there is only a slight decrease in the fast processes (A_1). The above results are in good agreement with the temperature-dependent original (Fig. S1) and normalized (Fig. 1c and d) PL intensity,

which is sufficient to confirm that the fast (A_1) and slow (A_2) decay processes stem from the transition of free exciton (X and IX) and defect-localized excitons (X_{def} and IX_{def}) respectively. Therefore, the schematic of exciton transition process in the WSe₂-WS₂ heterostructure can be shown as Fig. 2e. Additionally, the fitting results of lifetime (Fig. S2b and d) reveal that the fast decay lifetime τ_1 is ~ 1 ns and ~ 6 ns, which is consistent with the previously reported X and IX lifetime ranges²⁶, while the slow decay lifetime τ_2 is ~ 1200 ns and ~ 1700 ns, which should correspond to the defect-localized excitons¹⁷. It is worth noting that the increase in the lifetime of the slow process with the increase of temperature might be the unique properties of the defect-bound excitons. This is in contrast to the previously reported dark state-brightness caused by the splitting of the conduction band in tungsten selenide²⁷. Because of the separation of electrons and holes into different layers for interlayer excitons, both fast and slow decay lifetimes of IX_{def} are longer than that of X_{def} . It demonstrates that defect-localized exciton is a very feasible means to improve the radiative transition lifetime and offer a promising platform for the future valleytronic device.

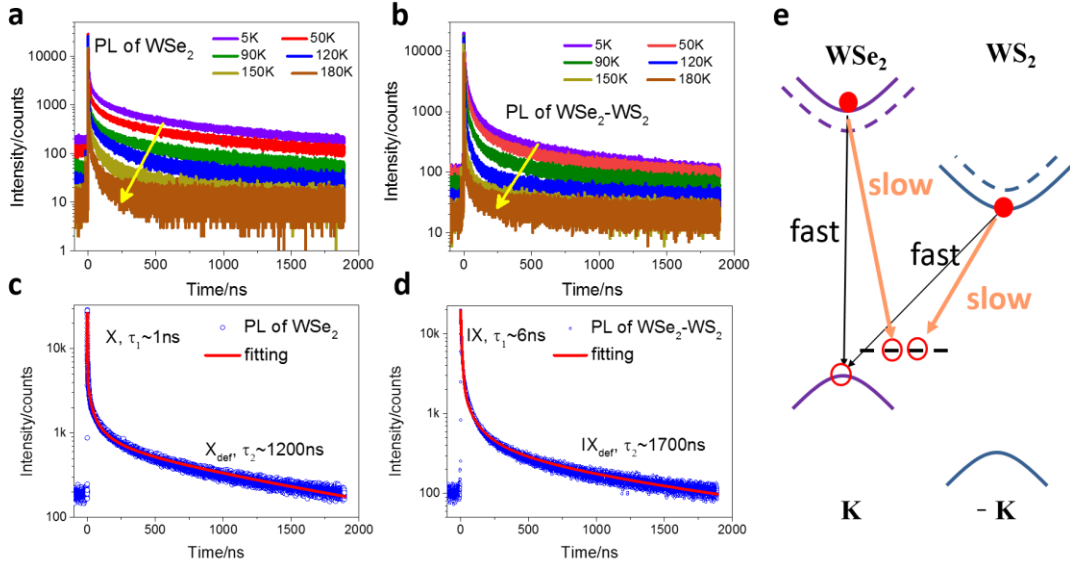


Fig. 2 Time-resolved PL and schematic of transition process of defect related excitons in AB-stacked WSe₂-WS₂ heterostructure. a and b, Time-resolved PL of monolayer WSe₂ (a) and WSe₂-WS₂ heterobilayer (b) at different temperature. c and d, Experimental (blue dots) and fitting (red lines) time-resolved PL of monolayer WSe₂ (c) and WSe₂-WS₂ heterobilayer (d) at temperature 5K. e, Diagram of transition process of defect related excitons in AB stacking WSe₂-WS₂ heterostructure. The excitation wavelength of pulse laser is at 670nm with repetition 500 KHz.

Magnetically-tunable valley polarization of defect-localized excitons.

As we know, because the valley polarization is one core figure of merit in the valley dynamics²⁸⁻³⁰, efficient modulation of the valley polarization has great significance. The valley or PL polarization can be defined as

$$P_{\pm} = \frac{I(\sigma_{\pm}) - I(\sigma_{\mp})}{I(\sigma_{\pm}) + I(\sigma_{\mp})}, \quad (2)$$

where $I(\sigma_{\pm})$ presents the σ_{\pm} detected polarization-resolved PL intensity. In order to evaluate the magnetic field response of valley polarization of the defect-localized

excitons, we first measured the steady-state PL spectra in detection with σ^- and σ^+ polarization as a function of out-of-plane magnetic field (B_z) and wavelength under σ^+ excitation as shown in Fig. 3a and b (the spectra under σ^- excitation shown in S3a and b).

Comparing the polarization-resolved PL spectra (Fig. 3a and b, Fig. S3a and b), it can be clearly observed that although the attenuation dynamics of IX_{def} and X_{def} have many similarities (Fig. 2a and b), their valley polarization and magnetic field response are quite different. The PL intensity of IX_{def} is sensitive to the magnitude but independent of the direction of the B_z . In detail, the PL in the detection with opposite circular polarization to the pumped one (excitation: σ^+ , detection: σ^- ; excitation: σ^- , detection: σ^+) is significantly enhanced with the increase of the weak B_z ($< \pm 0.4\text{T}$) and then becomes saturated with the further increase of the magnetic field. Nevertheless, the PL in the detection with the same polarization to the pumped one (excitation: σ^+ , detection: σ^+ ; excitation: σ^- , detection: σ^-) is on the contrary whose intensity becomes lower with larger magnetic field ($> \pm 0.4\text{T}$). On the contrary, the polarization-resolved PL of X_{def} is dominated by the direction of B_z . In Fig. 3a and b, the σ^+ and σ^- detected components of the X_{def} with σ^+ excitation changes monotonously with B_z but the trend is reversed.

According to the definition of valley polarization (Eq 2), we can quantitatively calculate the valley polarization of the defect-localized excitons. Figure 3c shows the calculated degree of valley polarization of IX_{def} as a function of B_z and wavelength with σ^+ excitation (the one with σ^- excitation shown in S3c). What makes this especially remarkable is that the polarization of IX_{def} possesses a negative value and can be significantly enhanced by a weak B_z ($< \pm 0.4\text{T}$), as shown a dark line around 0T in Fig. 3c and Fig. S3c. From the averaged polarization of IX_{def} (Fig. 3e) extracted from Fig. 3c and S3c, we can clearly observe that the steady-state valley polarization of IX_{def} presents a “ Λ ”-like dependence on the weak B_z . We calculate the slope of Fig. 3e to be about 0.4/KGs. Such a high magnetic sensitivity indicates that the IX_{def} possesses an unique (external field regulation) advantage in the application of the valley electronics device. In sharp contrast to IX_{def} , The measured data of the valley polarization of X_{def} (Fig. 3d and S3d) is obviously dominated by the direction of B_z ($> \pm 1\text{T}$). From the averaged results (Fig. 3f) extracted from Fig. 3d and S3d, the B_z tuning dependent PL polarization presents an “X”-like tendency, which is similar to the research of free excitons³¹. The experimental valley polarization results reveal that the IX_{def} and X_{def} have an obviously different magnetic response and the defect-localized excitons possess some unique and unrevealed transition dynamics and merits comparing with delocalized excitons.

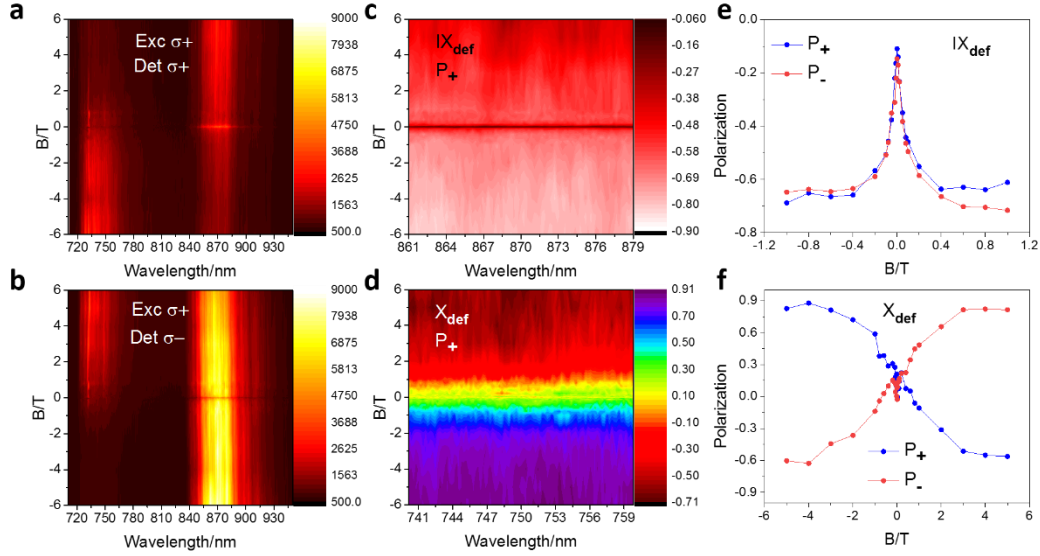


Fig. 3 Out-of-plane magnetic-field tunable PL intensity and polarization from IX_{def} and X_{def} in the AB-stacked $\text{WSe}_2\text{-WS}_2$ heterostructure. a and b, σ^+ (a) and σ^- (b) detected polarization-resolve PL spectrum as a function of out-of-plane magnetic field with σ^+ excitation at 670 nm wavelength. c and d, Out-of-plane magnetic field tuning polarization degree of IX_{def} (c) and X_{def} (d) with σ^+ excitation, respectively. e and f, The averaged valley polarization of IX_{def} (e extracted from Fig. 3c and S3c) and d and X_{def} (f extracted from Fig. 3d and S3d) as a function of B_z , respectively.

Magnetic tuning of the dynamics for IX_{def} in the heterostructure.

In order to understand above steady-state results (Fig. 3c and e), we need to figure out the possible dynamics of valley polarization for the defect-localized excitons. We perform the time-resolved measurements for both of the interlayer and intralayer defect-localized excitons with polarization resolution in the presence of different out-of-plane magnetic fields (B_z) using 670 nm pulse laser with repetition of 500 KHz. Fig. 4a shows the σ^+ (red cure) and σ^- (black cure) detected time-resolved PL of interlayer excitons (IX_{def} and IX) at selected B_z magnitudes with σ^+ excitation respectively (the one with σ^- excitation is referred to Fig. S4a). The measured results show that the slow decay process of the time-resolved PL detected in opposite polarization to the pumped one is obviously enhanced after applying a weak B_z . According to the definition of valley polarization in Eq. (2), we calculate the time-resolved valley polarization for interlayer excitons with σ^+ excitation at a selected weak B_z , as shown in Fig. 4b (the one with σ^- excitation is shown in Fig. S4b). Interestingly, it reveals that in the absence of B_z , the interlayer excitons have possessed a negative valley polarization at the beginning of the radiative recombination, which nevertheless quickly decay to nearly zero within the next few nanoseconds. Therefore, there is a small negative valley polarization (-10%) observed in the steady-state PL polarization (Fig. 3e). When adding a weak B_z within 0.4 T, we find that the slow decay process for the valley polarization is significantly enhanced. We fit the fast and slow processes in Fig. 4b and S4b with the bi-exponential decay

$$I(t) = (C_1 - C_2)e^{-\frac{t}{\tau_3}} + C_2e^{-\frac{t}{\tau_4}}, \quad (3)$$

where τ_3 and τ_4 are the valley lifetimes of the fast and slow decay, respectively, and C_1

and C_2 are the initial polarization of these processes. Fig. 4c show the fitting results of C_1 (purple dots) and C_2 (orange dots) with σ^+ excitation (the one with σ^- excitation is plotted in Fig. S4e). We can observe that C_2 shows a “ Λ ”-like tendency with the increase of B_z , but C_1 is nearly unchanged with B_z . Meanwhile, the slow decay lifetime (τ_4) shown in Fig. S4e becomes longer (even up to 3000ns at 0.4T) showing a “V”-like pattern with the increase of B_z , however, the fast decay lifetime (τ_3) shown in Fig. S4d is kept around 10 ns with a little fluctuation. According to Fig. 2b, we know that the fast process is originated from delocalized interlayer excitons (IX), but the slow process roots in defect-localized interlayer excitons (IX_{def}). Therefore, the enhanced slow process is responsible for the enhancement of the negative valley polarization in magnitude by the weak magnetic field in the steady-state measurements in Fig. 3. It indicates that the valley pseudospin of IX_{def} is more sensitive to the magnetic field (B_z) in comparison to the one of IX.

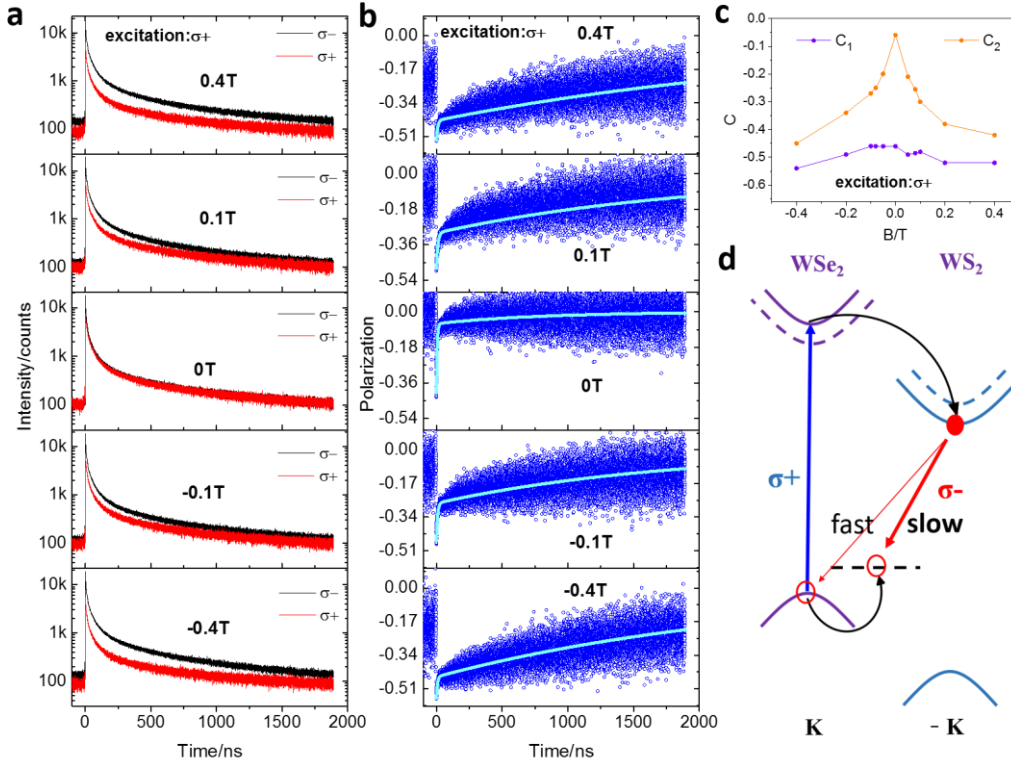


Fig. 4 The magnetic-field tunable time-resolved PL and valley polarization and schematics of transition dynamics of IX_{def}. a, Time- and polarization-resolved PL of WSe₂-WS₂ heterobilayer with σ^+ excitation at selected out-of-plane magnetic fields. b, Time-resolved PL polarization calculated from Fig. 4a at selected out-of-plane magnetic fields. The blue dots denote the experimental data and the light blue lines represent the fitting results. c, Fitting results of initial polarization of fast (C_1) and slow (C_2) process under σ^+ excitation respectively. d, Schematics of transition dynamics of IX_{def}.

The reversed or negative PL polarization of the interlayer exciton emerging in the AB-stacked heterobilayer was theoretically predicted by Y. Wang et al.³² and was observed experimentally very recently⁸. Similarly, we can also explain our observed

features for IX_{def} using the optical dipole of the interlayer exciton with kinematic momentum \mathbf{Q} , in which the electron and hole reside in the τK and $-\tau K$ valleys in the WS_2 and WSe_2 layer. The optical dipole operator \mathbf{D} is given by (derivation is referred to supplementary S6)

$$\begin{aligned} \mathbf{D}_{\tau K, -\tau K}(\mathbf{Q}) \approx & \Theta_I(\mathbf{r}=0) \langle \Psi_{\tau K, v} | \mathbf{D} | \Psi_{-\tau K, c} \rangle, \\ & + \frac{t_e}{E_I(\mathbf{Q}) - E_{\text{WSe}_2}} \langle 0 | \mathbf{D} | X_{\tau K} \rangle + \frac{t_h}{E_I(\mathbf{Q}) - E_{\text{WS}_2}} \langle 0 | \mathbf{D} | \Lambda_{-\tau K} \rangle \end{aligned} \quad (4)$$

The first term of the right-hand side denotes the direct recombination of the electron and hole in the WS_2 and WSe_2 monolayers with $\Psi_{-\tau K, c}$ and $\Psi_{\tau K, v}$ being their wavefunctions at the band edge. $\Theta_I(\mathbf{r}=0)$ represents the wavefunction of electron-hole relative motion in the interlayer exciton. The efficiency of the direct recombination is expected to be negligibly small due to the spatial separation of the electron and hole in different layers. The second term of the right-hand side comes from the interlayer hopping of the electron and the adjacent recombination of the intralayer exciton $X_{\tau K}$ in the WSe_2 layer, in which t_e is the interlayer hopping energy of the electron, $E_I(\mathbf{Q})$ and E_{WSe_2} are the energy of the interlayer and WSe_2 -layer excitons, respectively. This process does not cause the reversal of the PL polarization. While the third term of the right-hand side arises from the interlayer hopping of the hole and the adjacent recombination of the intralayer exciton $\Lambda_{-\tau K}$ in the WS_2 layer, in which t_h is the interlayer hopping energy of the hole and E_{WS_2} is the energy of the WS_2 -layer exciton. This process indeed causes the reversal of the PL polarization because the intralayer exciton $\Lambda_{-\tau K}$ in the WS_2 layer emits the PL with opposite polarization to that of $X_{\tau K}$ in the WSe_2 layer. Therefore, when the third process is dominant due to the more efficient interlayer hopping of the hole than the electron one, the PL polarization become reversed, as the observations in our experiments.

As a special case to possibly understand the relative magnitudes of the hopping energy, in the commensurate heterobilayer, t_e tends to be zero due to the interference effect during the electron hopping but t_h is still large³³. In reality, the lattice is not commensurate because the formation of interlayer exciton indicates a finite t_e , but the interlayer hopping of holes may still be more efficient than that of electrons as indicated by the first-principle calculation³². From this viewpoint, we attribute our measured negative PL polarization to the efficient interlayer hopping of hole that is also consistent with our interpretation on the magnetic-field sensitivity of the PL polarization, as we will discuss below. Thus, in Fig. 4d, consistent with Fig. 2b, the fast and slow processes can be understood according to the recombination of the intrinsic and defect-localized interlayer excitons due to the efficient interlayer hole hopping (more explanation is referred to supplementary S6).

From this viewpoint, any process that influences the interlayer hopping may influence the observation of the reversed PL polarization in the heterobilayer, e.g., the interface quality or motion between the two layers, that might make their observation in the experiment difficult. In particular, at the low temperature the weak localization of the hole arising from the quantum interference of different paths in the disordered WSe_2 layer by the W-defect inevitably influences the interlayer hopping of hole¹². By a small out-of-plane magnetic field, the interference of different paths of the hole become

destructive³⁴, and hence the weak-localization of the hole becomes less efficient and the interlayer hopping of the hole can play more important role in the optical dipole of the interlayer exciton [Eq.~(4)]. This can be responsible for the enhancement of the recombination of the defect-localized exciton to emit PL with opposite polarization that is sensitive to a weak magnetic field in the slow process (shown in Figs. 4b and c). Nevertheless, the fast process is less influenced by the weak magnetic field because the motion of the relatively free hole cannot be efficiently influenced by a weak magnetic field.

Magnetic tuning of the dynamics for X_{def} in WSe₂.

As addressed in Figs. 2d and f, we have seen that the B_z -tunable PL polarization of X_{def} presents an “X” pattern that is obviously different to the magnetic-field dependence of IX_{def} , suggesting their different transition dynamics. In order to figure out the microscopic process, we use the pulse laser (670 nm) to measure the time-and polarization-resolved PL of X_{def} at 10K. Fig. 5a shows the σ^+ (red) and σ^- (black) detected time-resolved PL spectra of X_{def} with different B_z under the σ^+ excitation (the one with σ^- excitation shown in Fig. S5a). The measurements reveal that the slow process of the PL detected in σ^- polarization become stronger than the one in σ^+ polarization when the B_z increases towards the positive magnitude. Whereas, this relation becomes reversed when B_z is reversed to the negative direction. Based on Fig. 5a, the time-resolved valley polarization of X_{def} under σ^+ excitation is plotted in Fig. 5b in the presence of different out-of-plane magnetic fields (the one with σ^- excitation is shown in Fig. S5b). Again, there exist the fast and slow processes for the time evolution of the PL polarization. We see that the magnitude of the PL polarization in the slow process is even larger than the initial PL polarization, implying the PL polarization becomes revived in the slow process even when it has been relaxed in the fast process. The revival of the PL polarization can be kept in a large magnitude (90%) without evident decay in a few microseconds. Moreover, the measured results show that the initial PL polarization is less influenced by the magnetic field, but the PL polarization becomes reversed in the slow process when the direction of B_z is reversed from the positive to the negative direction. Surprisingly, the reversed PL polarization is stabilized by the out-of-plane magnetic field in the negative direction that does not depend on the polarization of the excited state. This suggests that the PL polarization in the slow process is related to the distribution of exciton that is determined by the magnetic field³¹.

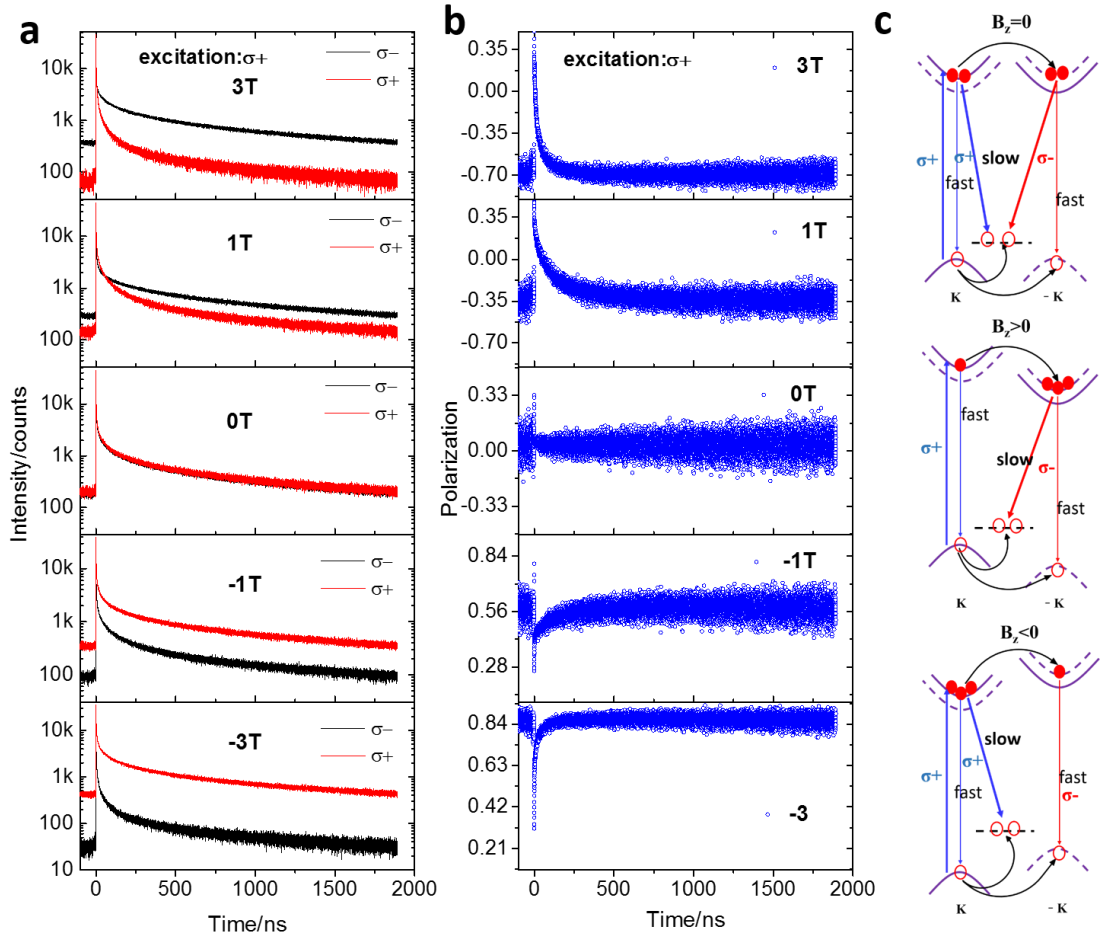


Fig. 5 Magnetic-field tunable time-resolved PL and valley polarization dynamics and schematic of valley dynamics of X_{def} . a, Time- and polarization-resolved PL of monolayer WSe_2 with σ^+ excitation at selected out-of-plane magnetic fields. b, Time-resolved PL polarization of monolayer WSe_2 with σ^+ excitation at selected out-of-plane magnetic fields. c, Schematic of valley dynamics of X_{def} under zero, positive and negative out-of-plane magnetic fields, respectively.

The physics here can be understood from the valley Zeeman effect³⁵⁻³⁶. Fig. 5c shows the diagram of transition dynamics of X_{def} under zero, positive and negative out-of-plane magnetic field. The fast process can be attributed to the intralayer free exciton with lifetime being sub-nanosecond that dominantly emits σ^+ (σ^-) light when pumped by σ^+ (σ^-) light. Hence, no valley polarization reversal happens at the fast process. The lifetime of the defect-localized intralayer exciton is extended to be hundreds of nanosecond or even microsecond, while its valley polarization lifetime is also in the order of microsecond, in consistent with the literature¹⁷. The long lifetime of these exciton allows to store the valley polarization because they experience weak optical dipole and electron-hole exchange interaction. We therefore attribute the slow process to the defect-localized intralayer exciton. The out-of-plane magnetic field then causes the valley Zeeman splitting of the defect-localized intralayer exciton that influences its quasi-equilibrium distribution. As shown in Fig. 5c, without the time-reversal symmetry broken by the magnetic field ($B_z=0\text{T}$), the equilibrium distribution of the defect-localized exciton tends to be the same that does not contribute to the PL

polarization in the slow process. A large magnetic field ($B_z > 1\text{T}$ and $B_z < 1\text{T}$) can cause a significant Zeeman splitting of these excitons in the two valleys, that then breaks the balance of these exciton populations in the two valleys by forming more low-energy exciton as indicated in middle and bottom panel of Fig. 5c. These low-energy exciton stores the valley polarization that can be even larger than the initial one with sign determined by the magnetic field direction. This explains the tunability of the valley polarization of the intralayer defect-localized exciton by the magnetic field in our experiment.

Discussion

In summary, we have investigated the tunable PL polarization dynamics of the defect-localized excitons by out-of-plane magnetic field in the AB-stacked WSe₂-WS₂ heterostructure. Several interesting features related to the defect-localized excitons can be extracted from our experiment. Firstly, both the interlayer and intralayer defect-localized excitons possess microsecond radiative and valley polarization lifetimes. Secondly, the PL polarization from the interlayer exciton is intrinsically negative and very sensitive to a weak out-of-plane magnetic-field ($< \pm 0.4\text{T}$) that can be significantly enhanced in magnitude by the weak magnetic field. Thirdly, the PL polarization from the intralayer exciton is determined by the direction of out-of-plane magnetic-field that can even revive by a strong out-of-plane magnetic-field ($> \pm 1\text{T}$) in the time evolution: the valley polarization increases up to 90% within few nanoseconds and then keeps this value in about few microseconds without attenuation. We explain that these defect related abnormal phenomena in the magnetic field dependence from the suppression of the localization of exciton and valley Zeeman effect. According to our work, defect-localized states of the TMDs heterostructure offer a broad and promising platform to extend the valley pseudospin lifetime and enrich the valley exciton physics.

Methods

Monolayer WSe₂ and WS₂ growth

We firstly grow the monolayer WSe₂/WS₂ through chemical vapor deposition (CVD). In detail, at upstream high-purity Se/S powder (Alfa Aesar, 36208/10785) of 0.2 g was added into a small quartz boat that served as the evaporation precursor. At downstream high-purity WO₃ powder (Alfa Aesar, 11828) of 10 mg was filled into another small quartz boat which was covered with the cleaned and facedown SiO₂/Si wafers (1.5 × 1.5 cm² in size) as the growth substrates. The whole system (the chamber and pipes) was evacuated by a mechanical pump to a base vacuum of ~4.5 Pa, and then followed by the re-filling of ultrahigh-purity argon gas (~99.999%) with a constant flow of 120 sccm. Under the protective environment of this carrier gas, the two heating zones of the tube furnace were ramped to target temperatures of 350/320 (for the Se/S powder) and 825 °C (for the WO₃ powder), respectively. From then on, the argon gas flow was turn down and kept at 60 sccm, and the growth was typically lasted for 30 min before being finally stopped by shutting off the power of the furnace. The substrate was naturally cooled down to room temperature before the cutoff of the argon flow and system venting.

WSe₂-WS₂ heterostructure transfer

We firstly spin-coated polymethyl methacrylate (PMMA) onto the growth WSe₂ substrate and dry

under 180 °C environment lasting 15min, and then gently soaked into the NaOH solution (2mol/L) about 60 min for etching the SiO₂ away and separating the PMMA/WSe₂ from substrate. After separation, clean the PMMA/WSe₂ using the deionized water very slowly and carefully. We fixed the WS₂/substrate on a rotatable platform and smoothly tiled the PMMA/WSe₂ onto a quartz window. At last, we stack the WSe₂-WS₂ heterostructure in AB order through rotating the WS₂ platform and moving the PMMA/WSe₂ quartz window under our homemade rotatable and high-resolution transfer platform system.

Time-resolved PL measurement

The attodry 1000 system was used to provide a low temperature (>4K) μ -PL spectrum testing platform. We employed the Clark MXR Impulse Laser to generate a 670 nm pulse laser with 500 KHz and pulse width less than 200ps and an electrical pulse as the start signal of the timer. We set up the circularity-resolved confocal μ -PL testing system and focus the 670 nm pulse laser using a 100x objective lens on the sample surface down to $\sim 1 \mu\text{m}$. The laser power on the sample was controlled at 20 μW for the excitation. The single photon detector (SPCM-AQRH-14) was used for collection and detection of the PL signals and switching the optical into electrical signals immediately, which was inputted into the timer as the end signal.

References

1. Mak, K. F.; Xiao, D.; Shan, J., Light–valley interactions in 2D semiconductors. *Nat. Photon.* **2018**, *12* (8), 451-460.
2. Xiao, D.; Liu, G. B.; Feng, W.; Xu, X.; Yao, W., Coupled spin and valley physics in monolayers of MoS₂ and other group-VI dichalcogenides. *Phys. Rev. Lett.* **2012**, *108* (19), 196802.
3. Yu, T.; Wu, M. W., Valley depolarization due to intervalley and intravalley electron-hole exchange interactions in monolayer MoS₂. *Phys. Rev. B* **2014**, *89* (20).
4. Rivera, P.; Yu, H.; Seyler, K. L.; Wilson, N. P.; Yao, W.; Xu, X., Interlayer valley excitons in heterobilayers of transition metal dichalcogenides. *Nat. Nanotechnol.* **2018**.
5. Rivera, P.; Seyler, K. L.; Yu, H.; Schaibley, J. R.; Yan, J.; Mandrus, D. G.; Yao, W.; Xu, X., Valley-polarized exciton dynamics in a 2D semiconductor heterostructure. *Science* **2016**, *351* (6274), 688-691.
6. Chen, H.; Wen, X.; Zhang, J.; Wu, T.; Gong, Y.; Zhang, X.; Yuan, J.; Yi, C.; Lou, J.; Ajayan, P. M.; Zhuang, W.; Zhang, G.; Zheng, J., Ultrafast formation of interlayer hot excitons in atomically thin MoS₂/WS₂ heterostructures. *Nat. Commun.* **2016**, *7*, 12512.
7. Jin, C.; Kim, J.; Utama, M. I. B.; Regan, E. C.; Kleemann, H.; Cai, H.; Shen, Y.; Shinner, M. J.; Sengupta, A.; Watanabe, K.; Taniguchi, T.; Tongay, S.; Zettl, A.; Wang, F., Imaging of pure spin-valley diffusion current in WS₂-WSe₂ heterostructures. *Science* **2018**, *360* (6391), 893-896.
8. Hsu, W.-T.; Lu, L.-S.; Wu, P.-H.; Lee, M.-H.; Chen, P.-J.; Wu, P.-Y.; Chou, Y.-C.; Jeng, H.-T.; Li, L.-J.; Chu, M.-W.; Chang, W.-H., Negative circular polarization emissions from WSe₂/MoSe₂ commensurate heterobilayers. *Nat. Commun.* **2018**, *9* (1).
9. Hanbicki, A. T.; Chuang, H. J.; Rosenberger, M. R.; Hellberg, C. S.; Sivaram, S. V.; McCreary, K. M.; Mazin, I.; Jonker, B. T., Double Indirect Interlayer Exciton in a MoSe₂/WSe₂ van der Waals Heterostructure. *ACS Nano* **2018**, *12* (5), 4719-4726.
10. Nagler, P.; Ballottin, M. V.; Mitioglu, A. A.; Mooshammer, F.; Paradiso, N.; Strunk, C.; Huber, R.; Chernikov, A.; Christianen, P. C. M.; Schuller, C.; Korn, T., Giant magnetic splitting inducing near-unity valley polarization in van der Waals heterostructures. *Nat. Commun.* **2017**, *8* (1), 1551.

11. Refaely-Abramson, S.; Qiu, D. Y.; Louie, S. G.; Neaton, J. B., Defect-Induced Modification of Low-Lying Excitons and Valley Selectivity in Monolayer Transition Metal Dichalcogenides. *Phys. Rev. Lett.* **2018**, *121* (16).
12. Zhang, S.; Wang, C. G.; Li, M. Y.; Huang, D.; Li, L. J.; Ji, W.; Wu, S., Defect Structure of Localized Excitons in a WSe₂ Monolayer. *Phys. Rev. Lett.* **2017**, *119* (4), 046101.
13. Song, S. H.; Joo, M.-K.; Neumann, M.; Kim, H.; Lee, Y. H., Probing defect dynamics in monolayer MoS₂ via noise nanospectroscopy. *Nat. Commun.* **2017**, *8* (1).
14. Hong, J.; Hu, Z.; Probert, M.; Li, K.; Lv, D.; Yang, X.; Gu, L.; Mao, N.; Feng, Q.; Xie, L.; Zhang, J.; Wu, D.; Zhang, Z.; Jin, C.; Ji, W.; Zhang, X.; Yuan, J.; Zhang, Z., Exploring atomic defects in molybdenum disulphide monolayers. *Nat. Commun.* **2015**, *6*, 6293.
15. He, Y. M.; Clark, G.; Schaibley, J. R.; He, Y.; Chen, M. C.; Wei, Y. J.; Ding, X.; Zhang, Q.; Yao, W.; Xu, X.; Lu, C. Y.; Pan, J. W., Single quantum emitters in monolayer semiconductors. *Nat. Nanotechnol.* **2015**, *10* (6), 497-502.
16. Koperski, M.; Nogajewski, K.; Arora, A.; Cherkez, V.; Mallet, P.; Veuillen, J. Y.; Marcus, J.; Kossacki, P.; Potemski, M., Single photon emitters in exfoliated WSe₂ structures. *Nat. Nanotechnol.* **2015**, *10* (6), 503-6.
17. Moody, G.; Tran, K.; Lu, X.; Autry, T.; Fraser, J. M.; Mirin, R. P.; Yang, L.; Li, X.; Silverman, K. L., Microsecond Valley Lifetime of Defect-Bound Excitons in Monolayer WSe₂. *Phys. Rev. Lett.* **2018**, *121* (5).
18. Wang, K.; Huang, B.; Tian, M.; Ceballos, F.; Lin, M. W.; Mahjouri-Samani, M.; Boulesbaa, A.; Puretzy, A. A.; Rouleau, C. M.; Yoon, M.; Zhao, H.; Xiao, K.; Duscher, G.; Geohegan, D. B., Interlayer Coupling in Twisted WSe₂/WS₂ Bilayer Heterostructures Revealed by Optical Spectroscopy. *ACS Nano* **2016**, *10* (7), 6612-22.
19. Schaibley, J. R.; Rivera, P.; Yu, H.; Seyler, K. L.; Yan, J.; Mandrus, D. G.; Taniguchi, T.; Watanabe, K.; Yao, W.; Xu, X., Directional interlayer spin-valley transfer in two-dimensional heterostructures. *Nat. Commun.* **2016**, *7*, 13747.
20. Unuchek, D.; Ciarrocchi, A.; Avsar, A.; Watanabe, K.; Taniguchi, T.; Kis, A., Room-temperature electrical control of exciton flux in a van der Waals heterostructure. *Nature* **2018**, *560* (7718), 340-344.
21. Hong, X.; Kim, J.; Shi, S.-F.; Zhang, Y.; Jin, C.; Sun, Y.; Tongay, S.; Wu, J.; Zhang, Y.; Wang, F., Ultrafast charge transfer in atomically thin MoS₂/WS₂ heterostructures. *Nat. Nanotechnol.* **2014**, *9* (9), 682-686.
22. Li, T.; Li, M.; Lin, Y.; Cai, H.; Wu, Y.; Ding, H.; Zhao, S.; Pan, N.; Wang, X., Probing Exciton Complexes and Charge Distribution in Ink-slab-Like WSe₂ Homojunction. *ACS Nano* **2018**, *12* (5), 4959-4967.
23. Deilmann, T.; Thygesen, K. S., Interlayer Trions in the MoS₂/WS₂ van der Waals Heterostructure. *Nano Lett.* **2018**, *18* (2), 1460-1465.
24. Ross, J. S.; Wu, S.; Yu, H.; Ghimire, N. J.; Jones, A. M.; Aivazian, G.; Yan, J.; Mandrus, D. G.; Xiao, D.; Yao, W.; Xu, X., Electrical control of neutral and charged excitons in a monolayer semiconductor. *Nat. Commun.* **2013**, *4*, 1474.
25. Jiang, C.; Xu, W.; Rasmita, A.; Huang, Z.; Li, K.; Xiong, Q.; Gao, W. B., Microsecond dark-exciton valley polarization memory in two-dimensional heterostructures. *Nat. Commun.* **2018**, *9* (1), 753.
26. Rivera, P.; Schaibley, J. R.; Jones, A. M.; Ross, J. S.; Wu, S.; Aivazian, G.; Klement, P.; Seyler, K.; Clark, G.; Ghimire, N. J.; Yan, J.; Mandrus, D. G.; Yao, W.; Xu, X., Observation of long-lived interlayer excitons in monolayer MoSe₂-WSe₂ heterostructures. *Nat. Commun.* **2015**, *6*, 6242.

27. Zhang, X. X.; You, Y.; Zhao, S. Y.; Heinz, T. F., Experimental Evidence for Dark Excitons in Monolayer WSe₂. *Phys. Rev. Lett.* **2015**, *115* (25), 257403.
28. Schaibley, J. R.; Yu, H.; Clark, G.; Rivera, P.; Ross, J. S.; Seyler, K. L.; Yao, W.; Xu, X., Valleytronics in 2D materials. *Nat. Rev. Mater.* **2016**, *1* (11), 16055.
29. Lee, J.; Wang, Z.; Xie, H.; Mak, K. F.; Shan, J., Valley magnetoelectricity in single-layer MoS₂. *Nat. Mater.* **2017**, *16* (9), 887-891.
30. Zeng, H.; Dai, J.; Yao, W.; Xiao, D.; Cui, X., Valley polarization in MoS₂ monolayers by optical pumping. *Nat. Nanotechnol.* **2012**, *7* (8), 490-3.
31. Aivazian, G.; Gong, Z.; Jones, A. M.; Chu, R.-L.; Yan, J.; Mandrus, D. G.; Zhang, C.; Cobden, D.; Yao, W.; Xu, X., Magnetic control of valley pseudospin in monolayer WSe₂. *Nat. Phys.* **2015**, *11* (2), 148-152.
32. Yu, H.; Wang, Y.; Tong, Q.; Xu, X.; Yao, W., Anomalous Light Cones and Valley Optical Selection Rules of Interlayer Excitons in Twisted Heterobilayers. *Phys. Rev. Lett.* **2015**, *115* (18), 187002.
33. Jones, A. M.; Yu, H.; Ross, J. S.; Klement, P.; Ghimire, N. J.; Yan, J.; Mandrus, D. G.; Yao, W.; Xu, X., Spin-layer locking effects in optical orientation of exciton spin in bilayer WSe₂. *Nat. Phys.* **2014**, *10* (2), 130-134.
34. Lee, P. A.; Ramakrishnan, T. V., Disordered electronic systems. *Rev. Mod. Phys.* **1985**, *57* (2), 287-337.
35. Srivastava, A.; Sidler, M.; Allain, A. V.; Lembke, D. S.; Kis, A.; Imamoğlu, A., Valley Zeeman effect in elementary optical excitations of monolayer WSe₂. *Nat. Phys.* **2015**, *11* (2), 141-147.
36. Li, Y.; Ludwig, J.; Low, T.; Chernikov, A.; Cui, X.; Arefe, G.; Kim, Y. D.; van der Zande, A. M.; Rigosi, A.; Hill, H. M.; Kim, S. H.; Hone, J.; Li, Z.; Smirnov, D.; Heinz, T. F., Valley Splitting and Polarization by the Zeeman Effect in Monolayer MoSe₂. *Phys. Rev. Lett.* **2014**, *113* (26), 266804.

Acknowledgements

We acknowledge the financial support from the Ministry of Science and Technology of China (Grant 2016YFA0200600), the National Natural Science Foundation of China (Grants 11474260, 21573207, 11504359, 11504364, 11504359 and 11804332), the Anhui Initiative in Quantum Information Technologies (Grant AHY090200), and the Fundamental Research Funds for the Central Universities (Grant WK2060190084). T. Y. was supported by the Netherland Organization for Scientific Research (NWO). The authors also thank Prof. Jin Zhao and Mr. Xiang Jiang for their helpful discussion.

Author contributions

T. S. Li, N. Pan, and X. P. Wang designed and conducted this research. T. S. Li prepared all of the samples, and performed the experiments with the assistance of X. F. Cui, K. X. Zhang, J. Y. Liu, and Q. S. Meng. T. Yu and T. S. Li established the theoretical model in this work. T. S. Li, T. Yu, N. Pan and X. P. Wang analyzed the experiment data and co-wrote the paper. All authors contributed to the discussions.